Control of the Flexural Axis of a SUAS Wing with Piezoelectric Actuation

James Davis*

Air Force Research Lab, Munitions Directorate, Flight Vehicles Integration Branch, Eglin AFB, FL 32542, USA

and

Nam H. Kim†

Dept. of Mechanical & Aerospace Engineering, University of Florida, Gainesville, FL 32611, USA

Through aeroelastic effects, the various structural parameters of a wing can have significant effects on the flight dynamics of any size aerial vehicle. In this paper, the preliminary analysis of a proposed structural system is presented. An equivalent beam model of the structural system is derived using the finite element method. The derived relation is then used to show that the parameters of the equivalent beam can be manipulated through the novel implementation of piezoelectric actuation. With the feasibility of such a system demonstrated, further research into the relationship between generalized structural parameters of a wing and the flight mechanics/dynamics of the complete vehicle is proposed and discussed.

Nomenclature

E	Young's modulus
Ω	Electric field
I	Area of Inertia
G	shear modulus
$\mathbf{K}$	Stiffness Matrix
S	Elastic Compliance Matrix
L	Span Length
c	Chord Length
A	Area
t	Thickness
$\mathbf{F}$	Force
$\mathbf{M}$	Moment
$\mathbf{T}$	Torque
$d_{i,j}$	Piezoelectric Strain Coefficients
ϵ	Material Strain
σ	Material Stress
i	Element Index
Subscript	
a	Actuator
LE	Leading Edge
TE	Trailing Edge

*Research Engineer/Graduate Student, Member AIAA, email:james.davis4@eglin.af.mil.

†Associate Professor, Associate Fellow AIAA, email:nkim@ufl.edu

I. Introduction

Aeroelasticity, as a discipline, is primarily concerned with the determination of stability limits and definition of the boundaries of the flight envelope. Some researchers have suggested that with the appropriate structural parameters, aeroelastic effects could be leveraged advantageously in the interior of the flight envelope to improve disturbance rejection.[1,2] It has also been suggested that the ability to manipulate the structural parameters in flight could be used to selectively enhance maneuvering capability through aeroelastic coupling.[3] These operational concepts of inherent stability and manipulating parameters for maneuverability are complementary to one another in that they each offer solutions to the others short comings, yet they are not mutually exclusive.

The concept of manipulating structural parameters has been pursued by researchers in the past which primarily focusing on conventional scale aircraft structures, one example of which can be found in Kota at al.[4] While some novel and theoretically sound concepts were proposed, this report serves as an illustration that conventional scale aircraft structural configurations with built up semi-monocoque designs do not readily lend them-selves to manipulation due too high stiffness and complicated interdependencies.

It is generally accepted that the flexibility of a wing structure tends to hinder maneuvering performance. Maneuverability being dependent on wing loading and inherent, or passive, stability requires motions and deformations to be in a decremental direction when prompted by an increase in loading thereby limiting the maximum attainable. Conventionally, to maximize maneuverability advanced control schemes are leveraged to allow smaller inherent stability margins or even inherent instability, there in maximizing the availability of wing loading. Unfortunately these advanced control schemes are expensive to develop and implement which prevents them from being adequately cost effective for lower cost vehicles. More relevant to the topic of this paper is the low inherent stability margins or instability tends to make the vehicle more susceptible to atmospheric disturbances in turn driving further complexity into the control scheme.

It is logical that the lower the initial values of the structural parameters the more pronounced the ability to influence their values will become. Therefore starting with a design intended to have significant inherent stability through deformations and implementing a methodology where a pertinent parameter could be changed at an appropriate time dramatic improvements in maneuvering performance could be realized through the aeroelastic coupling of the entire system. Pursuing this concept will enable the optimization of the structural system towards two conditions simultaneously instead of selecting one over the other to the detriment of both.

The long term goal of this research is to explore the expanded design space resulting from the union of these concepts and the implications on flight dynamics. In this paper we show that the design goal is achievable by presenting the preliminary analysis of a structural system that is capable of changing the structural parameters, primarily of which is the location of the flexural axis.

A. Formulation

As stated in multiple aeroelastic text books,[5–7] there are four prominent structural parameters which determine the aeroelastic response of a wing structure: bending stiffness, twisting stiffness, the location of the flexural axis, and the mass distribution. The structural configuration utilized in this work is similar to that discussed by Bisplinghoff[5] for development of models for aeroelastic wind tunnel testing. This configuration provides the ability to adjust the bending, twisting stiffness, and the location of the flexural axis relatively independent of one another. The full structure is presented in Figure 1 with a subsection highlighted in a free body diagram that will be used for this preliminary analysis.

Using the finite element formulation in symbolic form the linear Euler-Bernoulli beam element, a representation of the structure was assembled using Mathematica.[8] The essential boundary conditions are applied at the root nodes constraining them to fixed positions in the inertial frame. For the two other nodes, deformations in the span-wise and chord-wise directions are restricted as well as rotations about the vertical axis. Application of these boundary conditions reduces the stiffness matrix entries to the degrees-of-freedom of interest which are those associated with the vertical bending and spanwise twisting of the assembly. The stiffness matrix is then further reduced by enforcing that the twist angle of the fore and aft spars (elements

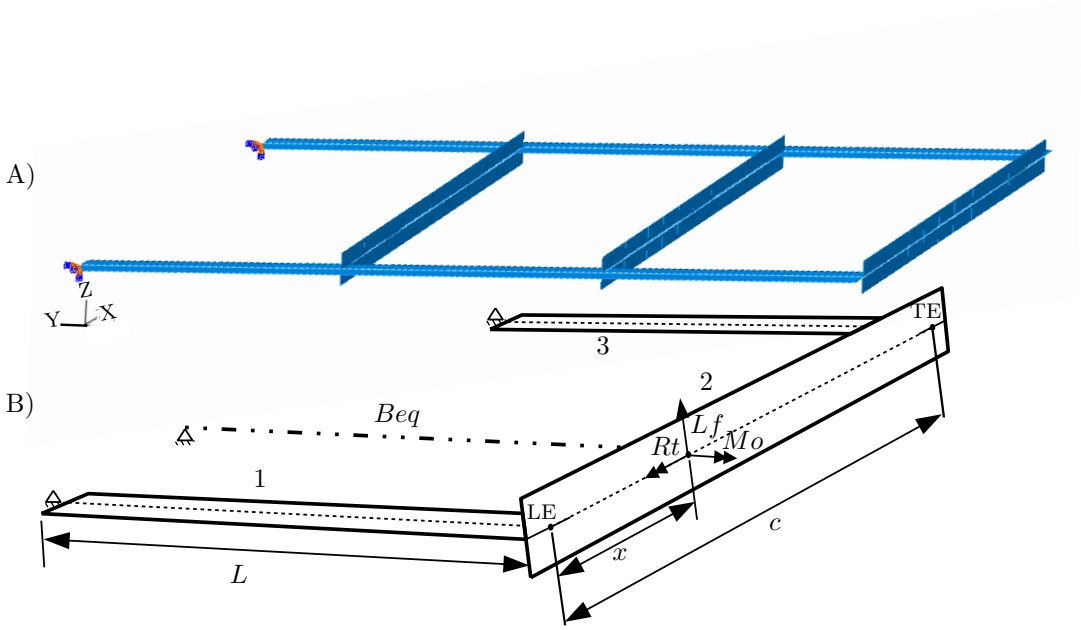

Figure 1. A) Proposed structural configuration and B) representative subsection and free body diagram.

1 and 3) be equal through the application of a transformation matrix as with standard finite element practices.[9] The stiffness matrix of the structure resulting from these simplifications is presented ~~in Eq. (1)~~

$$\mathbf{K} = \begin{pmatrix} y11+y21 & 2y22 & -y12 & -y21 & 0 \\ 2y22 & s1+s3+2y23+2y24 & 0 & -2y22 & 0 \\ -y12 & 0 & s2+y13 & 0 & -s2 \\ -y21 & -2y22 & 0 & y21+y31 & -y32 \\ 0 & 0 & -s2 & -y32 & s2+y33 \end{pmatrix} \tag{1}$$

Where $yi1 = \frac{12EiI_i}{Li^3}, yi2 = \frac{6EiI_i}{Li^2}, yi3 = \frac{4EiI_i}{Li}, yi4 = \frac{2EiI_i}{Li}$, and $si = \frac{GiKi}{Li}$ with i being the element number, and I_i being the area inertia associated with bending in the vertical direction. The corresponding degrees of freedom are $\begin{pmatrix} w_{LE} & \theta_{rib} & \theta x_{LE} & w_{TE} & \theta x_{TE} \end{pmatrix}^T$ which are the vertical displacement of the leading edge node, rotation of the rib about the Y axis, rotation of the leading edge node about the X axis, vertical displacement of the trailing edge node, and rotation of the trailing edge node about the X axis respectively.

Using the extended shape functions associated with the Euler-Bernoulli beam element, Eq. (**??**), the nodal equivalent forces for an applied point load, Lf, at a distance x from the leading edge, after applying the previously mentioned transformation matrix, are

$$\mathbf{F}(x) = \begin{pmatrix} \frac{Lf(c-x)^2(c+2x)}{c^3} & \frac{Lfx\left(c^2-3cx+2x^2\right)}{c^2} & 0 & \frac{Lf(3c-2x)x^2}{c^3} & 0 \end{pmatrix}^T \tag{2}$$

Using standard practices and the same shape functions, the equivalent nodal forces due to an applied point moment, Mo,at a distance x from the leading edge are

$$\mathbf{M}(x) = \begin{pmatrix} \frac{6Mox(-c+x)}{c^3} & \frac{Mo\left(c^2-6cx+6x^2\right)}{c^2} & 0 & \frac{6Mox(c-x)}{c^3} & 0 \end{pmatrix}^T \tag{3}$$

And for completeness, the equivalent nodal forces due to an applied point torque, Rt, along the rib, or element 2, at a distance x from the leading edge are calculated using linear interpolation functions

$$\mathbf{T}(x) = \begin{pmatrix} 0 & 0 & \frac{Rt(c-x)}{c} & 0 & \frac{Rtx}{c} \end{pmatrix}^T \tag{4}$$

These applied forces, F, Mo, and Rt are shown in Figure 1B. From the geometry in Figure 1B it is observed that the area of inertia term, I_2, for element 2, is far greater than that of the spar beams for bending in the Z direction. This is leveraged for further simplification purposes by assuming that the value of I_2 approaches infinity in the inverted stiffness matrix, thus making the rib analytically rigid in the vertical direction

$$\mathbf{K_{red}}^{-1} = \lim_{I_2 \to \infty} \mathbf{K}^{-1} \tag{5}$$

Applying the nodal equivalent forces from the point load to the simplified inverted stiffness matrix gives the relation between the displacements and rotations of the leading and trailing edge nodes to the relevant structural properties as well as the magnitude and location of the various loads applied at the point x along element 2 as measured from the leading edge.

$$\begin{pmatrix} w_{LE} & \theta_{rib} & \theta x_{LE} & w_{TE} & \theta x_{TE} \end{pmatrix}^T = \mathbf{K_{red}}^{-1} \cdot (\mathbf{F}(x) + \mathbf{M}(x) + \mathbf{T}(x)) \tag{6}$$

1. *Flexural Axis*

The flexural axis is defined as the location through which an applied vertical force will not cause a rotational displacement of the wing structure about the span-wise axis. The rotational displacement about the span-wise axis, θ_{rib}, as a function of the applied force, Lf, the location of application, x, and structural properties, is found from Eq.(6) with $Mo = Rt = 0$

$$\theta_{rib} = \frac{L^3 Lf(4EI_1 + (1 + E_{ratio})Ls2)(-c + x + E_{ratio}x)}{12c^2 EI_1(EI_1 + (1 + E_{ratio})Ls2) + (1 + E_{ratio})L^3(4EI_1 + (1 + E_{ratio})Ls2)(s2 + s3)} \tag{7}$$

where $E_{ratio} = \frac{EI_1}{EI_3}$.

To find the location of the flexural axis along the rib, Eq. (7) is set equal to zero and solved for $\frac{x}{c}$. This gives the location of the flexural axis as a function of the structural properties, as a fraction of the chord length

$$x_{fa} = \frac{x}{c} = \frac{EI_3}{EI_1 + EI_3} \tag{8}$$

This result is identical to what would be obtained with classic analysis methods for indeterminate structures. Eq. (8) can be rearranged to find the required stiffness ratio for a desired value of x_{fa}

$$E_{ratio} = \frac{EI_1}{EI_3} = \frac{1}{x_{fa}} - 1 \tag{9}$$

2. *Equivalent Beam*

To find the compliance matrix of an equivalent single beam representation of the structure, Beq as shown in Figure 1B, the three force vectors previously derived are evaluated as applied at the flexural axis location and summed. The sum of the forces is then multiplied into the simplified inverted stiffness matrix, determining the nodal displacements. Then, the calculated nodal displacements are linearly interpolated to the flexural axis location

$$\begin{pmatrix} w_{eq} \\ \theta x_{eq} \\ \theta y_{eq} \end{pmatrix} = \begin{pmatrix} \frac{c - cx_{fa}}{c} & 0 & 0 & \frac{cx_{fa}}{c} & 0 \\ 0 & 0 & \frac{c - cx_{fa}}{c} & 0 & \frac{cx_{fa}}{c} \\ 0 & 1 & 0 & 0 & 0 \end{pmatrix} \cdot \mathbf{K_{red}}^{-1} \cdot (\mathbf{F}(cx_{fa}) + \mathbf{T}(cx_{fa}) + \mathbf{M}(cx_{fa})) \tag{10}$$

Finally, the compliance matrix,$\mathbf{C_{eq}}$, for the equivalent single beam, Beq, is found by factoring out the point loads Lf, Rt, and Mo. This compliance matrix represents two of the four structural parameters, bending stiffness and twisting stiffness, discussed in section A as being significant in the determination of the aeroelastic behavior of the wing.

$$\begin{pmatrix} w_{eq} \\ \theta x_{eq} \\ \theta y_{eq} \end{pmatrix} = \mathbf{C_{eq}} \begin{pmatrix} Lf \\ Rt \\ Mo \end{pmatrix} \tag{11}$$

$$\mathbf{C_{eq}} = \begin{bmatrix} \frac{L^3}{3(EI_1+EI_3)} & \frac{L^2}{2(EI_1+EI_3)} & 0 \\ \frac{L^2}{2(EI_1+EI_3)} & \frac{L}{EI_1+EI_3} & 0 \\ 0 & 0 & \frac{(1+E_{ratio})L^3(4EI_1+(1+E_{ratio})Ls2)}{12c^2EI_1(EI_1+(1+E_{ratio})Ls2)+(1+E_{ratio})L^3(4EI_1+(1+E_{ratio})Ls2)(s1+s3)} \end{bmatrix} \quad (12)$$

The established relationships among the structural parameters of axis location and stiffness values form the basis of the manipulation methodology discussed in section B.

3. Non-Linear Validity

The relations of the flexural axis location and the equivalent beam model, C_{eq}, to the stiffness values for the original structure presented above are based on linear theory. The validity of extrapolating these relations to a geometrically nonlinear regime was investigated using commercially available finite element software package Abaqus and the structural configuration of Fig. 1B. The range of applied force and moments was selected by increasing the magnitude of the forces until significant geometrically nonlinear deformations were observed. These results serve as a preliminary investigation and are not intended to be all encompassing or inclusive of the entire range of loading conditions in application. The parameters used for the Abaqus analysis are presented in Table 1.

The axis location estimated from the linearly derived Eq. (8) was evaluated by comparison to nonlinear results extracted from the Abaqus analysis ~~by~~ applying the same load normal to the chord at 12.5%, 25% and 50% of the chord length. The load applied was a follower type, and as such remained normal to the rib throughout the deformation reminiscent of an aerodynamic pressure. The total load applied was $0.3lb$ in a linear ramp across each step, the results were interpolated to common values across all the steps and are presented here as a percentage of the total. The resulting rotation about the span-wise axis was taken as a function of the location of the load application and the zero intercept was found. Values for the zero intercepts are presented in Table 2 for various loading levels and the estimated value from Eq. (8). The results are also presented in Fig. (2), illustrating the process as well as the agreement between the linear and non-linear formulations.

Table 1. Values of structural parameters

	Length(in)	Height(in)	Width(in)	I(in^4)	E(psi)
Leading Edge Spar	7	0.015	0.5	1.4063E-07	21465585.2
Trailing Edge Spar	7	0.01	0.5	4.1667E-08	214[illegible]5.2
Rib	6	0.5	0.015	1.5625E-04	21465585.2

Table 2. Flexural Axis Calculation Results

Load:	5%	10%	15%	25%	50%	75%	100%	Est Eq. (8)
$\frac{x}{c}$:	0.228503	0.228511	.228544	.228790	.229616	.231819	.235579	.228570

From the nonlinear analysis, it was also found that the axis location varied less than .1% of the chord length over the deflection range investigated.

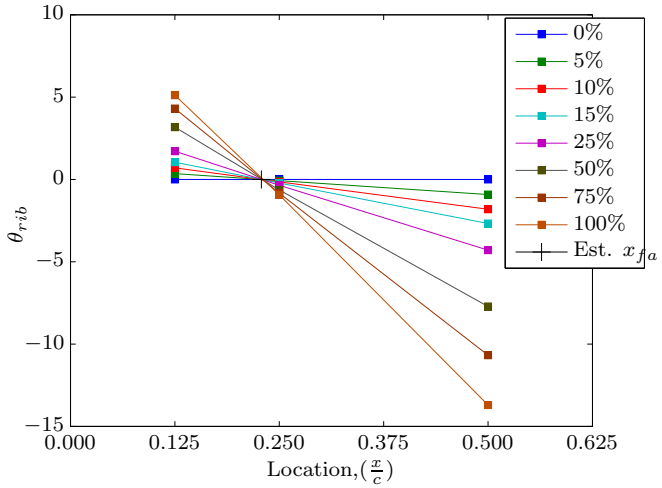

Figure 2. Results calculated by Abaqus showing the rotation of the rib (in degrees) due to the location of load application and magnitude as a percentage of the maximum; and the estimated location of x_{fa} from Eq. (8)

The equivalent single beam compliance matrix of Eq. (11), is based on linear theory and resulted from condensing the representative structure. Future work will be based on the assertion that the structural system can be represented as a single beam, *Beq*, placed at the flexural axis. To evaluate the validity of this assertion an analysis of the representative structure was conducted, again using Abaqus, by applying a vertical force, a chordwise torque and a spanwise moment to the model at the estimated location of the flexural axis using the stiffness parameters and estimated axis location shown in Tables 1 and 2. The results of this analysis, presented in figure 3, show significant agreement between the linear estimates and the non-linear analysis for all three cases of vertical force, chordwise torque and spanwise moment across the range investigated for the three degrees of freedom.

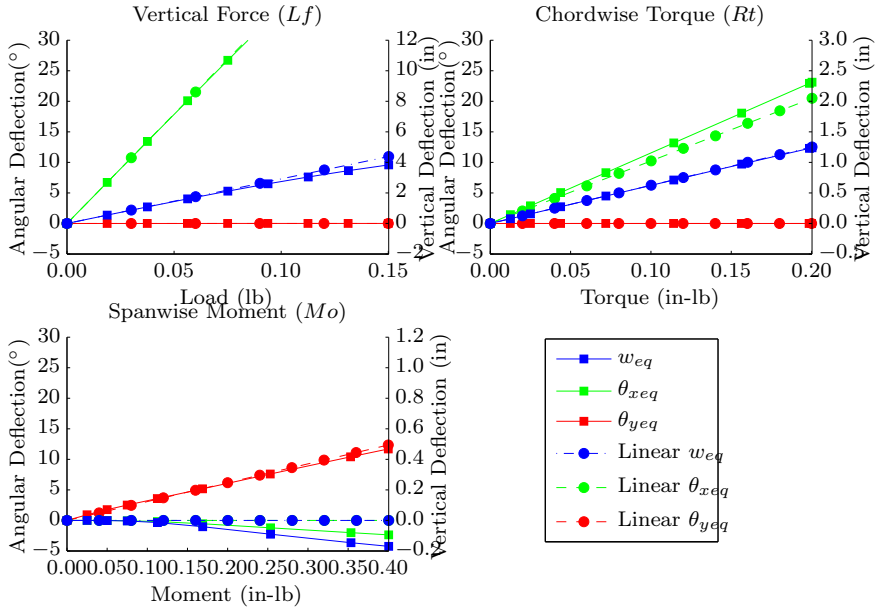

Figure 3. Comparison of nonlinear analysis and linear estimates from Eq. (11). The vertical deflections of w_{eq} are plotted against the secondary y axis.

The only discrepancy observed that might be of concern is the behavior due to the application of a span-wise moment where the nonlinearities results in a twist-bend coupling at moderate deflections. The significance of this discrepancy is application dependent and should be evaluated as part of the implementation process.

B. Axis Control

Manipulation of the location of the flexural axis, as well other stiffness parameters, is accomplished by the novel implementation of piezoelectric actuation in combination with a strain-dependent feed-back loop. Many past efforts to implement strain inducing actuators for control effector purposes[10–16] focused on geometric metrics such as degrees of rotation or distance of deflection. The design paradigm utilized to arrive at the presented design is to leverage the significant force producing capabilities of piezoelectric actuators, instead of the limited geometric displacements, and define the metric of interest as a change in properties of the structural system.

For a beam like device there are in general three possible actuation degrees of freedom, extension/contraction, bending and twisting. Any of these three could potentially be applied to any of the members of the structural system and all possibilities were considered. The design paradigm implemented focuses on effecting the stiffness parameters of a structural system. With that in mind, the simplified structural model presented in equations (8) and (11) can be used to provide insight into which actuation mechanism will have significant effects and where they should be implemented.

Since extensional stiffness parameters, EA, do not appear in the simplified model, extension/contraction actuation can be eliminated. Torsional stiffness parameters of $s1$,$s2$ and $s3$ only appear in the torsional term of Eq. (11). It follows that if it is desirable that the torsional stiffness be the only parameter controlled then a twisting actuator could be applied to any of the members.

The bending stiffness parameters are present in all terms involved, the simplest of which are the displacement and bending terms of Eq. (11) where a change in either EI_1orEI_3 would yield the same result. From Eq. (8) it is observed that a positive change in the axis location, moving it further aft, would require either a decrease in the EI_1 term or an increase in the EI_3 term. From the above analysis, to decrease the stiffness of a member would require a negative gain. In turn, this inversion would induce an actuation moment in the direction of the deforming force, feeding back into its self forming a divergent control loop or requiring the use of a more complex control logic. Increasing the EI_3 term utilizes the simple feedback loop in a stable manner and moves the axis location in the desired direction. From this conceptual analysis a bending type actuation is selected to be applied to the rear spar.

The active member is first derived as an isolated cantilever beam, and is then incorporated into the structure. The piezoelectric actuator is attached to the isolated cantilever beam in a mono-morph configuration. The strain of the beam is calculated at the root of the beam using standard finite element practices and shape functions associated with the Euler-Bernoulli beam element. A model of the feedback loop making the actuation voltage proportional to the calculated strain, and therefore displacement, is then developed. The feedback loop model is then combined with the original cantilever-beam stiffness matrix into an effective stiffness matrix with values proportional to the gain parameter. A state-space block diagram of the feedback loop is shown in Figur

The integrated structure/actuator model is based upon classic linear piezoelectric theory where the strain induced by the actuator is linearly dependent on the elastic properties of the loaded material and the applied electric potential field

$$\epsilon a_i = S_{ij}^E \sigma_j + d_{ij} \Omega \tag{13}$$

S_{ij}^E is the compliance matrix obtained under constant Electric field, and d_{ij} are the piezoelectric constants.

There are generally two configurations for a beam-like piezoelectric actuator, mono-morph and bi-morph. In a mono-morph configuration a layer of piezoelectric material is attached to only one side of the substrate, where in a bi-morph configuration piezoelectric layers are attached to the top and bottom of the substrate.

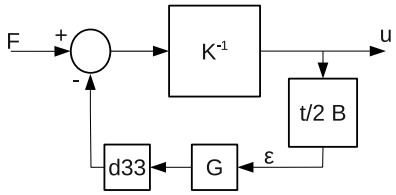

Figure 4. Feed Back Loop incorporated into structural system making piezoelectric actuation a function of displacement.

In both configurations a moment is induced via the piezoelectric effect by inducing an internal stress/strain at some distance from the neutral axis of the assembly and constant along the length of the actuator. A mono-morph expands and contracts on one side of the substrate while in a bi-morph the two actuators work together, one extending while the other contracts. While a bi-morph is more effective[17] a mono-morph is used here for simplicity. Assuming the neutral axis is at the geometric center of the assembly, the induced moment for a mono-morph actuator is proportional to geometric parameters, appropriate piezoelectric constants, and an applied Electric field field.[17]

$$M_a = \frac{t}{2} A_a d_{33} E_a \Omega \tag{14}$$

As discussed in Inman and Cudney,[17] incorporating the linear actuation model and finite element formulation results in a simple relation between the internal forces, applied forces, stiffnesss and displacements.

$$\mathbf{K} \cdot \mathbf{u} + \mathbf{F_a} = \mathbf{F} \tag{15}$$

where $\mathbf{u} = \begin{pmatrix} w_1 & \theta_1 & w_2 & \theta_2 \end{pmatrix}^T$, $\mathbf{F}$ is a vector of external applied forces, $\mathbf{K}$ the stiffness matrix for the entire assembly, and $\mathbf{F_a}$ is the vector of generalized internally applied forces due to actuation, Eq (16).

From implementation of the boundary conditions, with the actuator spanning the length of the beam, the vector of generalized internally applied forces due to actuation is

$$\mathbf{F_a} = M_a \frac{dN(L)}{dx} = \begin{pmatrix} 0 & 0 & 0 & 1 \end{pmatrix}^T M_a \tag{16}$$

where *N(x)* is a vector of the Euler-Bernoulli beam shape functions.

Again, assuming the neutral axis is at the geometric center of the beam, the strain displacement relation at the root, $x = 0$, is found from the curvature displacement relation, $B(x)$, and the total thickness t.

$$\epsilon = \frac{t}{2} B(0) \cdot \mathbf{u} = \begin{pmatrix} -\frac{3t}{L^2} & -\frac{2t}{L} & \frac{3t}{L^2} & -\frac{t}{L} \end{pmatrix} \cdot \mathbf{u} \tag{17}$$

A gain parameter, G, is set as the relation between the measured strain and the applied Electric field

$$\Omega = G\epsilon \tag{18}$$

Combining equations 14 -18 and simplifying, results in the internal force vector becoming a function of the displacement

$$\begin{aligned} \mathbf{F_a} &= \frac{1}{2} A_a d_{33} E_a G\, t \begin{pmatrix} 0 & 0 & 0 & 1 \end{pmatrix}^T \cdot \begin{pmatrix} -\frac{3t}{L^2} & -\frac{2t}{L} & \frac{3t}{L^2} & -\frac{t}{L} \end{pmatrix} \cdot \mathbf{u} \\ &= A_a d_{33} E_a G\, t^2 \begin{pmatrix} 0 & 0 & 0 & 0 \\ 0 & 0 & 0 & 0 \\ 0 & 0 & 0 & 0 \\ -\frac{3}{2L^2} & -\frac{1}{L} & \frac{3}{2L^2} & -\frac{1}{2L} \end{pmatrix} \cdot \mathbf{u} \end{aligned} \tag{19}$$

Combining the beam stiffness matrix, $\mathbf{K}$, with the applied internal force, $\mathbf{F_a}$, Eq. (15) becomes an effective stiffness matrix with values dependent on the gain parameter, G

$$\mathbf{Ka}(G) \cdot \mathbf{u} = \mathbf{F} \tag{20}$$

$$\mathbf{Ka}(G) = \begin{pmatrix} \frac{12EI}{L^3} & \frac{6EI}{L^2} & -\frac{12EI}{L^3} & \frac{6EI}{L^2} \\ \frac{6EI}{L^2} & \frac{4EI}{L} & -\frac{6EI}{L^2} & \frac{2EI}{L} \\ -\frac{12EI}{L^3} & -\frac{6EI}{L^2} & \frac{12EI}{L^3} & -\frac{6EI}{L^2} \\ -\frac{3\left(-4EI+A_a d_{33} E_a G t^2\right)}{2L^2} & \frac{2EI-A_a d_{33} E_a G t^2}{L} & \frac{3\left(-4EI+A_a d_{33} E_a G t^2\right)}{2L^2} & \frac{8EI-A_a d_{33} E_a G t^2}{2L} \end{pmatrix} \tag{21}$$

Electric field, Ω, is a function of the applied voltage and depends, in piezoelectric applications, on the geometry and spacing of the electrodes. Using Macro Fiber Composite (MFC) piezoelectric actuators as a base line, $\Omega = Ep/es$ where $es = 0.0197in$ is the electrode spacing and Ep is the applied voltage. Electrical limits of +1500V to -500V are imposed on the MFC actuators due to failure in the form of dielectric breakdown making the limits on the electrical field $76200V/in < \Omega < -25400V/in$. These limits must be taken into account when selecting a range of possible values for the gain parameter, G, so as to avoid overloading and failure in the form of dielectric breakdown and arcing.

Incorporating the effective stiffness matrix, $\mathbf{Ka}(G)$, into the analysis of Section 1 as the stiffness matrix of the trailing edge spar, element 3, an active version of the reduced compliance matrix, $\mathbf{Ca}(G) = {\mathbf{K_{red}}}^{-1}(G)$, is found. This active compliance matrix is then used in the same way as the passive variant to find the the location of the active flexural axis, ax_{fa}.

$$ax_{fa} = \frac{x}{c} = \frac{EI_1\left(16EI_3^2 + 4EI_3(Ls2 + PA) + 3LPAs2\right) + EI_3 Ls2(4EI_3 + PA)}{2EI_1^2(8EI_3 + 2Ls2 - PA) + EI_1\left(16EI_3^2 + 4EI_3(2Ls2 + PA) + LPAs2\right) + EI_3 Ls2(4EI_3 + PA)} \tag{22}$$

where the piezoelectric actuation term $PA = A_a d_{33} E_a G\, t^2$. It is noted that when $G = 0$, Eq (8) is recovered.

Rearranging Eq (8) for EI_3 and substituting this into Eq (22) gives the location of the active flexural axis relative to the passive location.

$$ax_{fa} = \frac{x}{c} = \frac{-3LPAs2 + (5LPAs2 - 4(PA + Ls2)EI_1)\, x_{fa} - 2\left(LPAs2 - 2PAEI_1 + 8EI_1^2\right) x_{fa}^2}{LPAs2\,(-1 + x_{fa}) - 16EI_1^2 x_{fa} + 2EI_1\left(PA - 2Ls2 - 4PAx_{fa} + 3PAx_{fa}^2\right)} \tag{23}$$

Using the location of the active flexural axis, ax_{fa}, and the active compliance matrix, $\mathbf{Ca}(G)$, an active version of the equivalent beam compliance matrix in Eq (11) can be derived.

$$\begin{pmatrix} w_{eq} \\ \theta x_{eq} \\ \theta y_{eq} \end{pmatrix} = \begin{pmatrix} \frac{c - cax_{fa}}{c} & 0 & 0 & \frac{cax_{fa}}{c} & 0 \\ 0 & 0 & \frac{c - cax_{fa}}{c} & 0 & \frac{cax_{fa}}{c} \\ 0 & 1 & 0 & 0 & 0 \end{pmatrix} \cdot \mathbf{Ca}(G) \cdot \left(\mathbf{F}\left(cax_{fa}\right) + \mathbf{T}\left(cax_{fa}\right) + \mathbf{M}\left(cax_{fa}\right)\right) \tag{24}$$

Just as above, the equivalent single beam compliance matrix, $\mathbf{Ca_{eq}}$, is found by factoring out the point loads Lf, Rt, and Mo.

$$\begin{pmatrix} w_{eq} \\ \theta x_{eq} \\ \theta y_{eq} \end{pmatrix} = \mathbf{Ca_{eq}}(\mathbf{G}) \begin{pmatrix} Lf \\ Rt \\ Mo \end{pmatrix} \tag{25}$$

Unfortunately, the active version of the equivalent compliance matrix is not as compact as the passive. The only zero entry is for the relation between the vertical force, Lf, and the spanwise rotation, θy_{eq} which was enforced by the value selected for ax_{fa}. Although the resulting matrix is not presented here the result shows that the proposed structural configuration and actuation system will enables the control of three aeroelastic parameters; the location of the flexural axis, the bending stiffness and twisting stiffness.

The active reduced compliance matrix, $\mathbf{Ca}(G)$, was implemented numerically. The assumptions concerning the location of the neutral axis in Eqs (b to b) was reassessed and a proper estimate of the location

was made using standard mechanics of materials practices. An analysis was conducted using the parameter values presented in Tables 1 to 2 with a constant point loading applied at 25% of the chord and various values for the gain. The range of gain values was determined by dividing the upper limit of Ω by the calculated strain from the applied vertical force with the structure in the passive state. The resulting deformation of the representative subsection is presented in Figure 5.

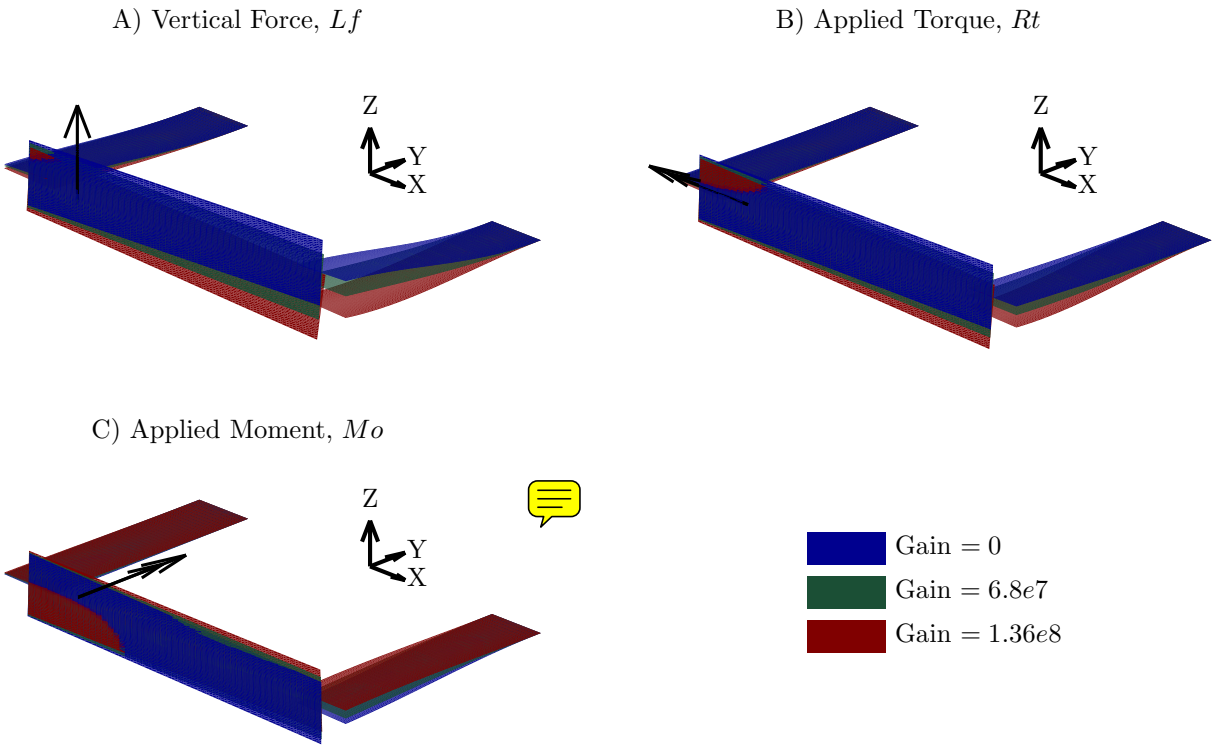

Figure 5. Structural system response to constant applied point (A)forces, (B)torques and (C)moments with various gain values.

From the figures it can be seen that increasing the gain parameter results in a reversal of the structural response. This phenomena can be explained in the context of the above analysis as the result of moving the flexural axis. When the axis is moved to the other side of the applied force the rotational deformation naturally changes direction. In application this change in structural response can be used as an control effector. With an increase in the gain, the axis moves aft which will effectively stiffen a flexible structure, making the vehicle more responsive, and if moved far enough can put the wing in a aeroelastically divergent configuration, where by the wing flares to higher twist angles proportionally to the wing loading and gain value. The commanded controlled divergence in turn generates a significant change in force distribution effectively using the entire wing as an control surface.

C. Discussion

A proposed structural system to simultaneously enable an increase in disturbance rejection and maneuvering performance by way of aeroservoelastic interactions was presented. The design of the proposed structural system was enabled by adoption of a novel actuation design paradigm, incorporating embedded actuators with the focus of affecting the stiffness metrics of a structure instead of the geometry.

It was shown that the proposed structural configuration can be represented as an equivalent beam located at the flexural axis. The ability of linear theory to estimate the location of the flexural axis in the geometrically nonlinear regime was assessed and shown to be consistently accurate.

The accuracy of a single linear beam representation of the structural system in terms of stiffness was assessed and a bend twist coupling resulting from geometrical nonlinearities was observed. The significance of this coupling effect is application dependent and would need to be assessed by incorporating the details of the vehicle to which it is being applied.

It was shown that incorporation of an embedded actuator acting along a beam in conjunction with a simple feedback loop based on a strain sensor results in the ability to change the effective stiffness of the beam by means of a gain parameter. Incorporating this active beam into the wing structure as the rear spar produces the ability to primarily change the location of the wing's flexural axis in flight as well as the representative stiffness parameters.

Future research will include an objective quantitative assessment of the relations between structural properties of a wing and flight mechanics/dynamics of the vehicle to include stability, disturbance rejection, and maneuverability.

References

[1]Ifju, P. G., Ettinger, S., Jenkins, D., and Martinez, L., "Composite Materials for Micro Air Vehicles," *SAMPE Journal*, Vol. 37, 2001, pp. 7–12.

[2]Ifju, P. G., Jenkins, D. A., Ettinger, S., Lian, Y., Waszak, M. R., and Shyy, W., "Flexible-Wing-Based Micro Air Vehicles," 2002, AIAA Paper 2002-0705.

[3]Livne, E., "Future of airplane aeroelasticity," *Journal of Aircraft*, Vol. 40, No. 6, 2003, pp. 1066–1092.

[4]Kota, S., Hetrick, J., and Saggere, L., "Design of a Variable Stiffness Spar," 1996.

[5]Bisplinghoff, R., Ashley, H., and Halfman, R., *Aeroelasticity*, Dover Publications, New York, NY, 1996.

[6]Dowell, E., Clark, R., Cox, D., Curtiss, H., Edwards, J., Hall, K., Peters, D., Scanlan, R., Simiu, E., Sisto, F., and Strganac, T., *A Modern Course in Aeroelasticity*, Kluwer Academic Publishers, 4th ed., 2004.

[7]Rodden, W. P., *Theoretical and Computational Aeroelasticity*, Crest Publishing, 2011.

[8]Wolfram Research Inc, *Mathematica*, Version 8.0, Champaign, Il, 2010.

[9]Cook, R., *Concepts and applications of finite element analysis*, John Wiley & Sons, fourth edition ed., 2002.

[10]Barrett, R., "Active aeroelastic tailoring of an adaptive Flexspar stabilator," *Smart Materials and Structures*, Vol. 5, 1996, pp. 723–730.

[11]Barrett, R., "All-moving active aerodynamic surface research," *Smart Materials and Structures*, Vol. 4, 1995, pp. 65–74.

[12]Barrett, R., "Aeroservoelastic DAP missile fin development," *Smart Materials and Structures*, Vol. 2, 1993, pp. 55–65.

[13]Ehlers, S. and Weisshaar, T., "Adaptive wing flexural axis control," *3rd International Conference on Adaptive Structures*, San Diego, Ca, 1993.

[14]Ehlers, S. and Weisshaar, T., "Effect of adaptive material properties on static aeroelastic control," Apr 13-15 1992.

[15]Ehlers, S. and Weisshaar, T. A., "Static aeroelastic behavior of an adaptive laminated piezoelectric composite wing," Apr 2-4 1990.

[16]Weisshaar, T. A. and Ehlers, S. M., "Adaptive aeroelastic composite wings–Control and optimization issues," *Composites Engineering*, Vol. 2, No. 5-7, 1992, pp. 457–476.

[17]Inman, D. and Cudney, H., "Structural and machine design using piezoceramic materials: a guide for structural design engineers," *Final Report to NASA Langley Research Center*, 2000.